

**DEVELOPMENT OF 3D PRINTED
ANTHROPOMORPHIC RADIOTHERAPY HEAD
PHANTOM USING KINECT® XBOX 360®
SCANNER**

NUR EMIRAH BINTI MOHD ZAIN

UNIVERSITI SAINS MALAYSIA

2021

**DEVELOPMENT OF 3D PRINTED
ANTHROPOMORPHIC RADIOTHERAPY HEAD
PHANTOM USING KINECT® XBOX 360®
SCANNER**

by

NUR EMIRAH BINTI MOHD ZAIN

**Thesis submitted in fulfilment of the requirements
for the degree of
Master of Science**

June 2021

ACKNOWLEDGEMENT

In the name of Allah who is most Merciful and most Generous, I would like to acknowledged and thankful to all who were involved directly or indirectly throughout my journey to complete my Master of Science in Medical Radiation (Radiotherapy).

I am very grateful to my main supervisor, Dr. Wan Nordiana Wan Abdul Rahman for all the advice and support during my study. I am also thankful to my co-supervisor, Dr. Wan Fatimah Wan Sohaimi for the assistance with the facilities access and guidance. Appraisement to Mr. Reduan Abdullah for assisting me in the workflow of the radiotherapy treatment planning system and irradiation of the phantoms. I am sincerely grateful to all the staff at the School of Health Sciences for their handful of favor in my research works. Special gratitude and appreciation to my mother, Ruzita Muhammad for all the love and emotional endorsement. To all my family and friends, thanks for the positive encouragement in my research journey.

Finally, I would like to give recognition to the School of Health Sciences Incentive grant, 1001/PPSK/AUPS001, and Research University Grant (RUI: 1001/PPSK/8012212) for funding my research equipment and materials. Thank you.

TABLE OF CONTENTS

ACKNOWLEDGEMENT	ii
TABLE OF CONTENTS	iii
LIST OF TABLES	vi
LIST OF FIGURES	vii
LIST OF SYMBOLS	xv
LIST OF ABBREVIATIONS	xvii
LIST OF APPENDICES	xx
ABSTRAK	xxi
ABSTRACT	xxiii
CHAPTER 1 INTRODUCTION	1
1.1 Research Background.....	1
1.2 Problem Statement and Novelty of the Study	2
1.3 Thesis Objectives	3
1.3.1 General Objective.....	3
1.3.2 Specific Objectives.....	3
CHAPTER 2 LITERATURE REVIEW	4
2.1 Radiotherapy	4
2.2 Radiotherapy Workflow	6
2.2.1 Diagnostic Imaging: Simulation	6
2.2.2 Treatment Planning	7
2.2.3 Quality Control: Pre-Treatment Verification	8
2.2.4 Treatment Delivery	9
2.3 Radiotherapy dosimetry	10
2.3.1 Ionization chamber (IC)	11
2.3.2 Radiochromic Film.....	12

2.3.3	Thermoluminescence Detector (TLD)	14
2.3.4	Optically Stimulated Luminescence (OSL)	15
2.3.5	Other Types of Dosimeter	16
2.4	Radiotherapy Phantom	18
2.5	Introduction to 3D Printing	21
2.6	Additive Manufacturing (AM) Radiotherapy Phantoms (AM-RPs).....	23
CHAPTER 3 MATERIALS AND METHODS		30
3.1	3D-Printed Head Phantom Fabrication	32
3.1.1	Image Acquisitions: Three-Dimensional (3D) Scanning	32
3.1.2	Image processing: Three-Dimensional (3D) Editing	36
3.1.3	Phantom Fabrication: Three-Dimensional (3D) printing	41
3.1.4	3D Printing Material: The Polylactic Acid (PLA)	43
3.1.5	Geometric Measurements and Weight	43
3.2	Phantom Dosimetry Characterization	45
3.2.1	Treatment Planning of RANDO® and 3D-Printed Phantom: Head and Neck Planning (Whole Brain Target Area: two Parallel Opposite-Field Beams)	45
3.2.2	GafChromic EBT3 Films Calibration	55
3.2.3	Thermoluminescence Detector (TLD) calibration	58
3.2.4	RANDO® Phantom Dose Assessment	62
3.2.4(a)	GafChromic EBT3 Films.....	62
3.2.4(b)	Thermoluminescence Detector (TLD).....	64
3.2.5	3D-Printed Head Phantom Dosimetry Evaluation	66
3.2.5(a)	GafChromic EBT3 Films.....	66
3.2.5(b)	Thermoluminescence Detector (TLD).....	69
CHAPTER 4 RESULTS AND DISCUSSION.....		71
4.1	The 3D-Printed Head Phantom Fabrication	72
4.1.1	Geometric Evaluation of 3D-Printed Head Phantom.....	72

4.1.2	CT Number (Hounsfield Unit) Analysis	77
4.2	Dosimetry Evaluation.....	79
4.2.1	Dosimeters Calibration.....	79
4.2.1(a)	GafChromic EBT3 Films Calibration.....	79
4.2.1(b)	Thermoluminescence Detector (TLD) Calibration.....	81
4.2.2	RANDO® Head Phantom.....	86
4.2.2(a)	GafChromic EBT3 Films Gamma Analysis	86
4.2.2(b)	Thermoluminescence Detector (TLD) Dose Evaluation	91
4.2.3	3D-Printed Head Phantom	94
4.2.3(a)	GafChromic EBT3 Films Analysis.....	94
4.2.3(b)	Thermoluminescence Detector (TLD) Dose Evaluation	95
4.3	Comparison Between 3D-Printed and RANDO® Head Phantom.....	98
4.3.1	Dosimetry Characterization using GafChromic EBT3 Films	98
4.3.2	Dosimetry Characterization using Thermoluminescence Detector (TLD).....	98

**CHAPTER 5 CONCLUSION, LIMITATIONS, AND FUTURE
RECOMMENDATIONS..... 99**

5.1	Conclusion.....	99
5.2	Limitations of The Study.....	100
5.3	Recommendations for Future Research	101

REFERENCES..... 102

APPENDICES

LIST OF PUBLICATIONS

TURNITIN SCREENING REPORT

LIST OF TABLES

	Page
Table 3.1	The beam information50
Table 3.2	The treatment unit information51
Table 3.3	The dose information51
Table 3.4	The dose-volume information52
Table 4.1	The slices measurements of 3D-Printed Head Phantom and RANDO® Head Phantom.....74
Table 4.2	Comparison of RANDO® and 3D printed head phantom weight76
Table 4.3	The data plotted from the calibration film process79
Table 4.4	The recorded data of PMT noise, light noise, and background noise from the TLD reader as quality control performance82
Table 4.5	The recorded data of 89 TLD-100 chips from the sensitivity test82
Table 4.6	The setting of passing criteria of gamma index.87
Table 4.7	The recorded data of PMT noise, light noise, and background noise from the TLD reader as quality control performance88
Table 4.8	The recorded data of PMT noise, light noise, and background noise from the TLD reader as quality control performance92
Table 4.9	The recorded data of 40 TLD-100 chips from the irradiation inside RANDO® Head Phantom.....92
Table 4.10	The recorded data of PMT noise, light noise, and background noise from the TLD reader as quality control performance96
Table 4.11	The recorded data of 40 TLD-100 chips from the irradiation inside 3D-Printed Head Phantom96
Table 5.1	HU of each slice of the 3D printed head phantom. Hu, Hounsfield units; Ar, area; Av, average CT value; SD, standard deviation; CT, computed tomography..... 114

LIST OF FIGURES

	Page	
Figure 1.1	Qualitative comparison of (a) an anthropomorphic phantom, the ‘patient’ in this example, and (b) the 3D printed model. Note in (b) the coronal and axial film planes can be seen in the 3D printed phantom which can be set by the clinician. Also, the slice section numbers of the anthropomorphic phantom are preserved in the 3D printed model, which is remarkable considering the phantom was scanned with 3 mm CT slice thickness. The figure is adapted from (Ehler et. al, 2014).....	2
Figure 2.1	The schematic diagram of a linear accelerator (LINAC). The figure is adapted from (Saeed, 2015).....	5
Figure 2.2	The schematic diagram of a radiotherapy workflow. The figure is adapted from (Osman, 2019).....	6
Figure 2.3	The Phillips SPECT-CT in the Nuclear Medicine, Radiotherapy & Oncology Department, Hospital Universiti Sains Malaysia, HUSM	7
Figure 2.4	The tools in the Monaco treatment planning system. This figure is adapted from (Clements, Schupp, Tattersall, Brown, & Larson, 2018)	8
Figure 2.5	The ArcCheck phantom with (a) and without (b) optional cavity insert. This figure is adapted from (Petoukhova, Van Egmond, Eenink, Wiggeraad, & Van Santvoort, 2011)	9
Figure 2.6	The cancer patients on the Varian LINAC treatment couch in the Nuclear Medicine, Radiotherapy & Oncology Department, Hospital Universiti Sains Malaysia, HUSM	10
Figure 2.7	The figure of the cylindrical ionization chamber. This figure is adapted from www.flukebiomedical.com	12

Figure 2.8	The figure of irradiated radiochromic film calibration strips (film batch lot b=#12171303). This figure is from (Palmer, 2015)	14
Figure 2.9	The figure of thermoluminescence detector chips in different sizes and shapes. This figure is from http://www.tld.com.pl/tld/index.html	15
Figure 2.10	The optically stimulated luminescence detector (a) and OSL reader (b). This figure is from (Okino et al., 2016; Remley, 2017)	16
Figure 2.11	Different Sensitivity Modulated Advanced Radiation Therapy (SMART) dosimeter designs. (a) A double-stack SMART dosimeter design with a gold nanoparticles (AuNps) doped compartment (clear) and undoped compartment (dyed yellow). (a') The same double-stack SMART dosimeter after exposure of half of it to ultraviolet radiation, showing the radiation-induced change in optical density. A transparent yellow dye was added to the undoped compartment to allow the 2 compartments to be visually distinguished. (b) The actual cylinder-in-cylinder SMART dosimeter was analyzed in this study after irradiation. Red arrows indicate the direction of irradiation.). This figure is from (Alqathami et al., 2012)	18
Figure 2.12	The figure of radiotherapy phantoms in different sizes and shapes depending on their category. This figure is from (Tino et al., 2019)	21
Figure 2.13	The figure of a type of 3D printer available online. This figure is from https://www.forbes.com	22
Figure 2.14	The methods in the production of 3D printed prototype model (Rengier et al., 2010).....	23
Figure 2.15	Comparison of the original patient CT scan registered with the completed phantom CT scan. Panels on the left show slices of the original patient CT scan, panels in the middle are from the CT scan of the assembled phantom, and panels on the right are the 3D-rendered models of the original patient and the phantom. (a) and (b) Compare axial slices, (c) and (d) compare coronal slices, and	

	(e) and (f) compare sagittal slices. (g) and (h) Compare rendered models of the phantom and patient CT scans, respectively. This figure is from (Yea et al., 2017).....	25
Figure 2.16	The process of a 3D-printed anthropomorphic patient-specific head phantom for patient-specific quality assurance of intensity-modulated radiotherapy. This figure is from (Yea et al., 2017).....	25
Figure 2.17	Top-down view of the cardiac phantom; the dotted line indicates the approximate location of the mitral annular plane if projected straight down into the model (A). A view of the right side of the second (identical) phantom; the dotted line indicates approximate planar location and diameter of the mitral annulus if projected straight into the model (B). A sectional view of the mitral annulus and calcification is seen from the left atrium (C). A sectional view of the mitral annulus and calcification is seen from the left ventricle (D). LV: Left Ventricle; LA: Left Atrium; RV: Right Ventricle; Ao: Aorta; PA: Pulmonary Artery (Izzo et al., 2016).....	26
Figure 2.18	The fabrication process of 3D printed customized bolus using a 3D scanner. (Park et al 2017).....	28
Figure 3.1	Schematic illustration of chapter 3 summarization.....	31
Figure 3.2	Schematic illustration of volumetric datasets acquisitions.....	33
Figure 3.3	The properties of Kinect® Xbox 360® scanner.....	33
Figure 3.4	The properties of Kinect® Xbox 360® scanner.....	33
Figure 3.5	3D-scanning image obtained (a) 0° (b) 45° (c) 270° (d) 360°.....	35
Figure 3.6	3D-scanning 3D-editing process (a) Watertight process (b) Move and crop process (c) Removing unwanted parts (d) Final-edit data...	36
Figure 3.7	The 3D-editing software used (a) Mudbox (b) 3D Builder (c) Sculpttris.....	37
Figure 3.8	The sketching of dosimeter slots from top slice to slice 9 for the internal editing process.....	39

Figure 3.9	(a) Slice-by-slice cutting process (b) Individual slice editing process for slot establishment (c) Top slice without slots at the upper surface (d) Top slice editing at a lower surface	40
Figure 3.10	The different view of slots editing process using Blender 3D software	40
Figure 3.11	(a) The slots in 3D data from Blender software of 3D printed phantom slice 1 (upper side) (b) The 3D Printed Phantom slice 1 and top slice (c) The slots from the upper side of the RANDO® phantom slice 1 (d) The slots from a lower side of slice 1, RANDO®	41
Figure 3.12	The MyVista Cube 200 3D printer	42
Figure 3.13	The image before final slices editing (a) Option one where the phantom is in the 100% solid object (b) The phantom printed in a shell form	42
Figure 3.14	(a) Illustration diagram of positioning and set up of printing (b) The density fills range	42
Figure 3.15	The X-value and Y-value used to measure the geometric of the phantom.....	44
Figure 3.16	The weight measurement of RANDO® and 3D printed phantom on the weighing platform scale device.....	44
Figure 3.17	CT simulation positioning; (a) Placing phantom firmly (b) Horizontal laser (c) Middle laser (d) Correct positioning phantom entered the CT head	46
Figure 3.18	CT topography images; (a) Frontal view (b) Sagittal view	46
Figure 3.19	CT simulation of 3D-Printed Head Phantom; (a) Right lateral laser positioning (b) Left lateral laser positioning (c) Central laser positioning (d) CT topography images	47
Figure 3.20	The contouring process of organ at risk (OARs) in the Oncentra TPS.....	48
Figure 3.21	The planning manager and calculation using the Oncentra TPS	48

Figure 3.22	The whole-brain target area as confirmed by MLC	49
Figure 3.23	The dose-volume histogram (DVH) graph analysis.....	49
Figure 3.24	(a) The back view of the 3D-Printed Head Phantom in Oncentra TPS (b) The lateral view (c) Treatment plan from RANDO® was used on 3D-printed phantom.....	53
Figure 3.25	The image registration in Oncentra TPS (a) The contouring of external skin (b) The contouring of right and left phantom holder (c) The planning target volume, PTV of the shape of the whole brain (d) The alternative view of PTV	54
Figure 3.26	(a) The parallel-opposed beam applied to the phantom CT image (b) The conformal of MLC to the shape of PTV (c) The dose prescribed at 400 cGy (d) The white line of 95% isodose coverage	54
Figure 3.27	GafChromic™ EBT3 film calibration; (a) The dose range (b) The position of 3 × 3 cm ² film (c) The calibration standard parameter ...	56
Figure 3.28	The six irradiated films with different dose ranges (0, 50 cGy, 100 cGy, 200 cGy, 300 cGy, 400 cGy, 500 cGy, and 600 cGy) placed in the EPSON Flatbed scanner	57
Figure 3.29	The pre-calibration curve formulates from FilCal software (a) The dose measured and the dose reading table (b) The same size ROI were drawn on the film (c) The graph of measured dose versus true dose	57
Figure 3.30	The summary of the films calibration (a) Films scanning (b) The reading of film dose in unit pixel value (c) Applying lookup-table to the film (d) The second reading of measured dose in Gy for the calibration curve initiation	58
Figure 3.31	(a) The TLDs in a calibration plate (b) The 10 × 10 cm ² field size irradiation set up (c) The schematic diagram of the calibration set up for sensitivity test (d) The positioning of solid water phantom on a table couch.....	61
Figure 3.32	(a) The annealing oven (b) The TLD reader couch.....	61

Figure 3.33	(a) (a) The TLDs in a plate (b) The TLDs experience annealing process (c) The TLD chip in the reader drawer (d) The reading of TL signal in a monitor screen.....	62
Figure 3.34	GafChromic™ EBT3 films preparation (a) The film was cut following the shape of phantom's slices using A4 paper (b) Punching two holes in the middle of the film for phantom holder insertion (c) The cut-off results of the films (d) Films placed in between the phantom's slices.....	63
Figure 3.35	(a) The films in between slices prepared for irradiation (b) The setup of phantom (c) The alignment of the phantom in compliance with the laser (d) The phantom ready to be irradiated	63
Figure 3.36	The arrangement of 40 TLD chips inside the RANDO® phantom ...	65
Figure 3.37	The adhesive tape sealed the slot hole to secure the chips from falling during irradiation	65
Figure 3.38	The positioning set up of RANDO® Head Phantom on the PRIMUS LINAC couch. (a) The phantom was supported by immobilization devices such as headrest and poly-b (b) The gantry was set to 90° degrees and 270° for left and right lateral beam (c) The laser intersects at the isocentre with the whole-brain target area	66
Figure 3.39	The EBT3 films preparation (a) The film was abridged following the shape of slices using A4 paper (b) Punching two holes in the middle of the film for phantom holder insertion (c) The upper view of the phantom (d) For stabilization, the printed phantom was sticking together with slice 10 of RANDO® phantom.....	67
Figure 3.40	(a) The films in between slices prepared for irradiation (b) The setup of the phantom (c) The alignment of the phantom in compliance with the laser (d) The phantom ready to be irradiated....	67
Figure 3.41	3D-Printed Head Phantom positioning set up (a) Set up using headrest A and poly B (b) Isocentre placement (c) Lateral laser localization (d) Orientation of x, y, and the x-axis of the couch.....	68

Figure 3.42	Films dimensioning in phantom (a) Slice 2 (b) Slice 3 (c) Slice 4 (d) Slice	69
Figure 3.43	The printed phantom wholly wrapped with adhesive tape (a) Left lateral view (b) Back view (c) Right lateral view (d) Front view	69
Figure 3.44	The arrangement of TLD chips in 3D-Printed Head Phantom (a) Slice 2 (b) Slice 3 (c) Slice 4 (d) Slice 5	70
Figure 3.45	The setup of the 3D-Printed Head Phantom on the LINAC couch....	70
Figure 4.1	The front and back view of the 3D-Printed Head Phantom.....	73
Figure 4.2	The right and left view of the 3D-Printed Head Phantom	73
Figure 4.3	Comparison side-by-side between the RANDO® Head Phantom with the 3D Printed Head Phantom (a) The frontal view (b) The right lateral view (d) The back view (d) The left lateral view	75
Figure 4.4	HU measurement of slice 3 of the 3D printed head phantom. Hu, Hounsfield units; Ar, area; Av, average CT value; SD, standard deviation; CT, computed tomography.....	78
Figure 4.5	The graph of netOD versus absorbed dose (cGy)	80
Figure 4.6	The net optical density per unit dose in intensity as a function of dose.	80
Figure 4.7	The scanned films after irradiation using Epson Flatbed scanner (a) The film under slice 1 (b) The film under slice 2 (c) the film under slice 3 (d) The film under slice 4	86
Figure 4.8	The scanned films after applied with lookup-table of the pre-calibrated curve (a) The film under slice 1 (b) The film under slice 2 (c) the film under slice 3 (d) The film under slice 4	87
Figure 4.9	The four image identification of gamma analysis on films located in between slice 1 and 2	89
Figure 4.10	The four image identification of gamma analysis on films located in between slice 2 and 3	89
Figure 4.11	The four image identification of gamma analysis on films located in between slice 3 and 4	90

Figure 4.12	The four image identification of gamma analysis on films located in between slice 4 and 5	90
Figure 4.13	The initial reading of films using Epson Flatbed scanner. (a) The film placed between slice 1 and 2 (b) The film placed between slice 2 and 3 (3) The film placed between slice 4 and 5.....	94
Figure 4.14	The repetition of film reading after a few alterations. (a) The film placed between slice 1 and 2 (b) The film placed between slice 2 and 3 (3) The film placed between slice 4 and 5.....	95
Figure 5.1	The overexposed of films after applying the lookup table. (a) The film placed between slice 1 and 2 (b) The film placed between slice 2 and 3 (3) The film placed between slice 4 and 5.....	117
Figure 5.2	The overexposed of films after applying the lookup table for the second time. (a) The film placed between slice 1 and 2 (b) The film placed between slice 2 and 3 (3) The film placed between slice 4 and 5	117

LIST OF SYMBOLS

MeV	Mega electron Voltage
AgBr	Silver Bromide
OD	Optical Density
μm	Micrometre
Lx	Lux
μC	micro Coulomb
LiF	Lithium fluoride
Mg	Magnesium
Ti	Titanium
AuNPs	Gold NanoParticles
kg	kilogram
Ft	Feet
In	Inches
Lb	Pound
cm	centimeter
r_m	Gamma positioning
mm	millimeter
HU	Hounsfield Unit
Gb	Gigabytes
Fpm	Frame per minutes
mm/s	millimetre per second
MU	Monitor Unit
D_{max}	Dose at maximum
Gy	Gray

cGy	centi Gray
MV	Mega Voltage
kV	kilo Voltage
I_0	Initial intensity
I	Intensity
$\rho_{e,w}$	mean relative electron density
P	mass density
Ar	Area
Av	Average
SD	Standard Deviations
AU	Anstronomical Unit
°	Degree
°C	Degree Celcius
pA	pAscal

LIST OF ABBREVIATIONS

IMRT	Intensity-Modulated Radiation Therapy
VMAT	Volumetric Modulated Arc Therapy
IGRT	Integrated-Guided radiation Therapy
SBRT	Stereotactic Body Radiation Therapy
3D	Three dimensional
CT	Computed Tomography
PLA	Poly-Lactic Acid
TLD	ThermoLuminescence Detector
RF	RadioFrequency
IAEA	International Atomic Energy Agency
NCI	National Cancer Institute
LINAC	Linear Accelerator
QC	Quality Control
IC	Ionization Chamber
OSL	Optically Stimulated Luminescence
SOP	Standard Operation Procedure
QA	Quality Assurance
PDD	Percentage Depth Dose
USA	United States of America
LET	Linear Energy Transfer
RBE	Relative Biological Effectiveness
MOSFET	Metal-Oxide-Semiconductor Field-Effect Transistor
SMART	Sensitivity Modulated Advanced Radiation Therapy
RP	Radiotherapy Phantoms
CT-ED	Computed Tomography-Electron Density
AM	Additive Manufacturing
IT	Informational Technology
CAD	Computer-Aided Design
ABS	Acrylonitrile Butadiene Styrene
ART	Alderson Radiation Therapy
ICRU	International Commission Radiation Units and Measurements

Inc	Incorporation
CTA	Computed Tomography Angiography
TPS	Treatment Planning System
LV	Left Ventricle
LA	Left Atrium
LAA	Left Atrial Appendage
Ao	Aorta
RV	Right Ventricle
RA	Right Atrium
DICOM	Digital Imaging and Communication in Medical
DD	Dose Difference
OAR	Organ at Risk
RPL	RadioPhotoLuminescence
USM	Universiti Sains Malaysia
HUSM	Hospital USM
STL	STereLithography
CPU	Central processor unit
RAM	Random-access memory
OBJ	Object
FDM	Fused-deposition method
FFF	Fused-filament fabrication
CD	Compact Disk
MLC	Multi-leaf collimator
DVH	Dose-volume histogram
AAA	Anisotropic Analytical Algorithm
RF	Radiofrequency
ARIA	Accessible Rich Internet Application
SSD	Source-to-surface distance
IEC	International Electrotechnical Commission
Iso	Isocentre
Rt	Right
Lt	Left
PTV	Planned Target volume
AAPM	American Association of Physicist in Medicine

FilCal	Film Calibration
ROI	Region of Interest
EMR	Electronic Medical Record
PMT	Photo-multiplier tube
ECC	Element Correction coefficient

LIST OF APPENDICES

Appendix A	PTW – Verisoft Of Gamma Analysis On Film Located Between Slices In RANDO® Head Phantom
Appendix B	International Seminar Medical Physicist (ISMP) 2019
Appendix C	International Seminar Medical Physicist (IsmP) 2019 – Oral Presentation
Appendix D	10 th International Conference On Isotopes (10 th Ici) 2020
Appendix E	10 th International Conference On Isotopes (10 th Ici) 2020 – Oral Presentation
Appendix F	18th South-East Asia Congress Of Medical Physics (Seacomp) 2020 (Virtual Meeting)
Appendix G	Table 5.1: Hu of Each Slice of The 3d Printed Head Phantom. Hu, Hounsfield Units; Ar, Area; Av, Average Ct Value; Sd, Standard Deviation; Ct, Computed Tomography
Appendix H	Correction Factors
Appendix I	Figure 5.1 and Figure 5.2 Overexposed (Darkening) Of Irradiated Films After Applying Lookup Table In 3d-Printed Head Phantom

PEMBANGUNAN FANTOM ANTROPOMORFIK KEPALA CETAKAN 3 DIMENSI MENGGUNAKAN PENGIMBAS KINECT® XBOX 360®

ABSTRAK

Tujuan radioterapi adalah untuk menyampaikan dos sinaran maut kepada sel kanser sambil mengekalkan kesihatan tisu normal. Jaminan kualiti sebelum rawatan sangat penting untuk memastikan penghantaran dos yang tepat dan ini biasanya dilakukan menggunakan standard fantom air atau fantom standard yang tidak mempunyai bentuk anatomi manusia. Oleh itu, penggunaan fantom khusus mengikut bentuk dan ciri-ciri pesakit adalah penting untuk mengelakkan kesilapan dosimetri semasa rawatan. Kajian ini melakukan penyiasatan ke atas penggunaan Kinect® Xbox 360® untuk membuat fantom kepala radioterapi antropomorfik menggunakan teknologi percetakan 3D. Penggunaan pengimbas 3D dan bukannya data tomografi berkomputer (CT) untuk mencipta fantom pada dasarnya adalah untuk mengelakkan pendedahan sinaran yang tidak perlu terutamanya apabila mengumpul imej permukaan pesakit. Pembangunan fantom dalam tesis ini terbahagi kepada dua fasa iaitu pembikinan fantom dan penilaian fantom. Pembikinan fantom bermula dengan melakukan imbasan 3D ke atas RANDO® kepala fantom yang mewakili kepala manusia menggunakan pengimbas Kinect® Xbox 360®. Imej yang diperolehi disunting dalam format 3D dan dipindahkan dalam format stereolitografi (STL) untuk percetakan 3D. Fantom dicetak menggunakan bahan asid polilaktik (PLA) dengan pengisian penuh. Selepas fantom kepala bercetak 3D berjaya dihasilkan, fantom tersebut melalui penilaian secara geometri dan secara dosimetri di samping membuat perbandingan dengan RANDO® kepala fantom. Saiz, bentuk dan berat fantom dibandingkan dengan fantom piawai dan hanya terdapat sedikit perbezaan iaitu $\pm 18\%$

dalam faktor perbezaan saiz dan 15% dalam faktor perbezaan berat. Unit Hounsfield (HU) kedua-dua fantom menunjukkan nilai ± 63.3 HU. Fantom kemudiannya menjalani simulasi CT dan perancangan rawatan telah dibina dengan kawasan sasaran seluruh otak menggunakan sistem perancangan rawatan Eclipse. Fantom kepala bercetak 3D serta RANDO® kepala fantom kemudiannya didedahkan kepada sinaran melalui perancangan rawatan yang dibina dengan dua jenis dosimeter iaitu filem TLD dan Gafchromic EBT3. Keputusan dosimetri untuk filem GafChromic EBT3 dalam fantom kepala bercetak 3D tidak menunjukkan dapatan yang baik tetapi berjaya mendapatkan analisis indeks gamma yang boleh diterima bagi RANDO® fantom. Kehadiran jurang udara di antara lapisan fantom secara khususnya adalah sebab utama mengapa indeks analisis gamma tidak dapat diselesaikan untuk fantom kepala bercetak 3D. Pengukuran dos menggunakan TLD menghasilkan keputusan yang hampir serupa untuk kedua-dua phantom. Oleh itu, fantom kepala bercetak 3D berjaya dibangunkan dengan imbasan 3D menggunakan alat yang lebih murah iaitu pengimbas 3D Kinect® Xbox 360® dan kebolehlaksanaan fantom dalam jaminan kualiti radioterapi adalah pragmatik berhubung dengan bentuk luaran struktur kepala. Hasil daripada kajian ini menunjukkan kebolehlaksanaan fantom bercetak 3D untuk aplikasi radioterapi dan dengan pengoptimuman lanjut, fantom mungkin disesuaikan dengan ciri-ciri anatomi manusia yang kompleks dan sifat dosimetri yang unggul.

**DEVELOPMENT OF 3D PRINTED ANTHROPOMORPHIC
RADIOTHERAPY HEAD PHANTOM USING KINECT® XBOX 360®
SCANNER**

ABSTRACT

Radiotherapy aims to deliver a highly lethal radiation dose to cancer while preserving the healthy normal tissue. Pre-treatment quality assurance is extremely important to ensure accurate dose delivery and this is usually performed using standard phantom that is lacking in specific human anatomy. Therefore, the application of patient-specific phantom is important to avoid dosimetric errors during treatment. This study investigates the application of Kinect® Xbox 360® scanner to fabricate anthropomorphic radiotherapy head phantom using 3D printing technology. The use of a 3D scanner instead of computed tomography (CT) data to create the phantom is principally to avoid unnecessary radiation exposure, especially when collecting the superficial contour image of the patient. The development of the phantom in this thesis consists of two phases which are phantom fabrication and phantom evaluation. The phantom fabrication started by performing 3D scanning of standard RANDO® head phantom which to represent human head using Kinect® Xbox 360® scanner. The images obtained were edited in 3D format and transferred in stereolithography (STL) format for 3D printing. The phantom was printed using polylactic acid (PLA) materials with full infill. After the 3D printed head phantom was completely fabricated, the phantom was geometrically and dosimetrically evaluated in comparison to the RANDO® head phantom. The phantom size and weight were compared to the standard phantom and only a slight difference of grossly $\pm 18\%$ in size difference and 15% in weight difference were recorded. Hounsfield unit (HU) of both phantoms shows the

value of ± 63.3 HU. The phantoms were later undergoing CT simulation and treatment planning was constructed with whole-brain target area using the Eclipse treatment planning system. The 3D printed head phantom, as well as RANDO® head phantom, was then irradiated as the constructed treatment planning with two types of dosimeters which were the TLDs and Gafchromic EBT3 films. The dosimetric results for GafChromic EBT3 films in the 3D printed head phantom did not show good results while acceptable gamma index analysis was obtained for RANDO® head phantom. The presence of the air gap in between the phantom slices is primarily the reason why the gamma analysis index cannot be completed for the 3D printed head phantom. The dose measurement using TLD produces almost similar results for both phantoms. Thereby, the 3D-Printed Head Phantom is successfully developed throughout the 3D scanning using a cheaper tool of Kinect® Xbox 360® scanner and the feasibility of the phantom in radiotherapy quality assurance is pragmatic with regards to the external shape of the head structure. The outcome from this study demonstrates the feasibility of a 3D printed phantom for radiotherapy application and with further optimization, the phantom might be customized with complex human anatomical features and superior dosimetric properties.

CHAPTER 1

INTRODUCTION

1.1 Research Background

The productions of additive manufacturing (AM) radiotherapy phantoms (AMRPs) in today's world is mostly by using 3D extraction from CT, angiography, or other 3D patient images. In this very study, the fabrication of the 3D-Printed Head Phantom was using Kinect® Xbox 360® scanner and it was printed using PLA materials. This study was pioneering in using such a scanner to 3D scan in AMRPs field compared to other studies made by previous research that are using more advanced optical scanners or 3D scanners. A different approach was made in this study besides the scanner used, instead of using patient's data, the 3D raw data of printed phantom was collected throughout the 3D scanning process of the RANDO® Head Phantom. The productions of 3D-Printed Head Phantom were printed using MyVista Cube 200 3D printer and later on, it was tested in dosimetry and geometry characteristics which then compared to the standard dosimetry and shape of RANDO® Head Phantom. The results were recorded and analyzed with references from other AMRPs studies for better understanding and in ensuring the quality of the printed phantom produced in terms of its practicality in clinical radiotherapy. Figure 1.1 shows an example of a 3D-Printed Head Phantom produced from a study by Ehler et al. (Ehler, Barney, Higgins, & Dusenbery, 2014)

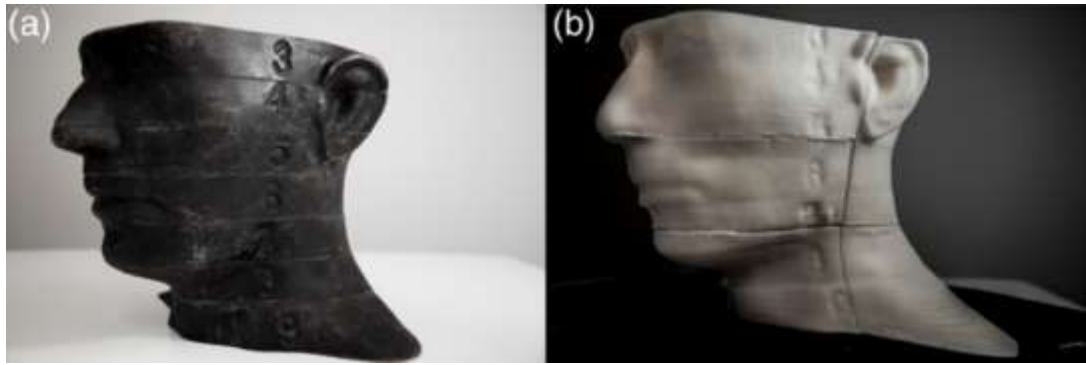


Figure 1.1 Qualitative comparison of (a) an anthropomorphic phantom, the ‘patient’ in this example, and (b) the 3D printed model. Note in (b) the coronal and axial film planes can be seen in the 3D printed phantom which can be set by the clinician. Also, the slice section numbers of the anthropomorphic phantom are preserved in the 3D printed model, which is remarkable considering the phantom was scanned with 3 mm CT slice thickness. The figure is adapted from (Ehler et. al, 2014)

1.2 Problem Statement and Novelty of the Study

The common issue that arises in radiotherapy is how to achieve accurate dosimetry for better treatment delivery to patients. Commonly, quality assurance was performed in radiotherapy to answer the dosimetric problem. However, current standard phantoms used are very extravagant, available only in standard size and shape, and not specific to the patient body which this will lead to dosimetric error as the phantom is not mimic humans especially the patients.

To develop a patient-specific radiotherapy phantom, the patient-external contour and internal organ need to be properly simulated. In this study, an anthropomorphic radiotherapy head phantom was constructed using 3D printing with PLA materials. The phantom is fabricated using a 3D scanner which is the Microsoft® Kinect® Xbox 360® scanner instead of using computed tomography (CT) scans which is complicated and delivers unwanted radiation exposure. The design of a phantom using a CT scan image also require heavy computation that might require more time to construct. Therefore, we investigate the potential use of Microsoft® Kinect® Xbox

360® scanner to produce a phantom model using 3D printing technology. Standard RANDO® phantom was utilized to represent the patient and as a dosimetric comparison to assess the clinical viability of this technique in radiotherapy.

1.3 Thesis Objectives

1.3.1 General Objective

To develop anthropomorphic radiotherapy head phantom using Kinect® Xbox 360® scanner.

1.3.2 Specific Objectives

- 1) To investigate the feasibility of the Kinect® Xbox 360® scanner in the 3D scanning of external human head anatomy complexes.
- 2) To fabricate the head phantom from 3D printing and to introduce a much cheaper phantom in comparison to the expensive commercial phantom for radiotherapy.
- 3) To assess the geometric and dosimetry accuracy of the head phantom.

CHAPTER 2

LITERATURE REVIEW

2.1 Radiotherapy

Radiotherapy is a treatment that applies radiation to kill cancer cells and it is one of the major types of cancer treatment other than chemotherapy and surgery. It uses ionizing radiation to destroy cancer cells and suppress cancer cell growth. The types of radiation used are photon or electron beams depend on whether the tumor is deep-seated inside the body or superficial around the skin. The energy of radiation used is higher than the one applied in diagnostic radiology where radiotherapy applies in megavoltage (MV) to kilovoltage (kV) energy, while radiology is only within the kV range of energy. The ionizing radiation is produced by a Linear Accelerator (LINAC) machine which comprises the main compartment of the stand which storing radiofrequency (Dipasquale, Poirier, Sprunger, Uiterwijk, & Miralbell) power generator inside, the x-ray tube that consists of an electron gun, accelerating waveguide, electron beam transport, 270° bending magnet and x-ray target located inside a gantry and a treatment couch as illustrated in Figure 2.1. Besides the LINAC machine, cobalt-60 is used in radiation therapy as a source of MV beams. (IAEA), 2020)

The radiotherapy professional consist of a team of qualified experts and experienced medical practitioners in radiation oncology which include medical doctors, medical physicists, and radiation therapy technologist. Radiotherapy can be delivered externally or internally. In external beam radiotherapy, radiation beams were delivered to the patients from the outside using LINAC while during internal radiation therapy, the radiation is delivered internally using a portable radiation source (IAEA), 2020). The types of cancer cells and where it is located are the main reason in choosing between the external beam radiotherapy and internal beam radiotherapy. External beam

radiotherapy is the practice of local treatment, which means it treats only a specific targeted area of the cancer cells. For example, if the patient has cancer at the right breast, then the radiation only will be projected to the patient's right chest, not the whole body.

Meanwhile, for internal radiation therapy or termed as brachytherapy, the source of radiation is put directly inside the patient's body. Brachytherapy uses a solid-state radiation source in a form of seeds, ribbons, and capsules that will be placed inside the patient's body, in or near the tumor. Similar to external beam radiation therapy, brachytherapy is also a local treatment and treats only a specific part of a patient's body. (NCI, 2019).

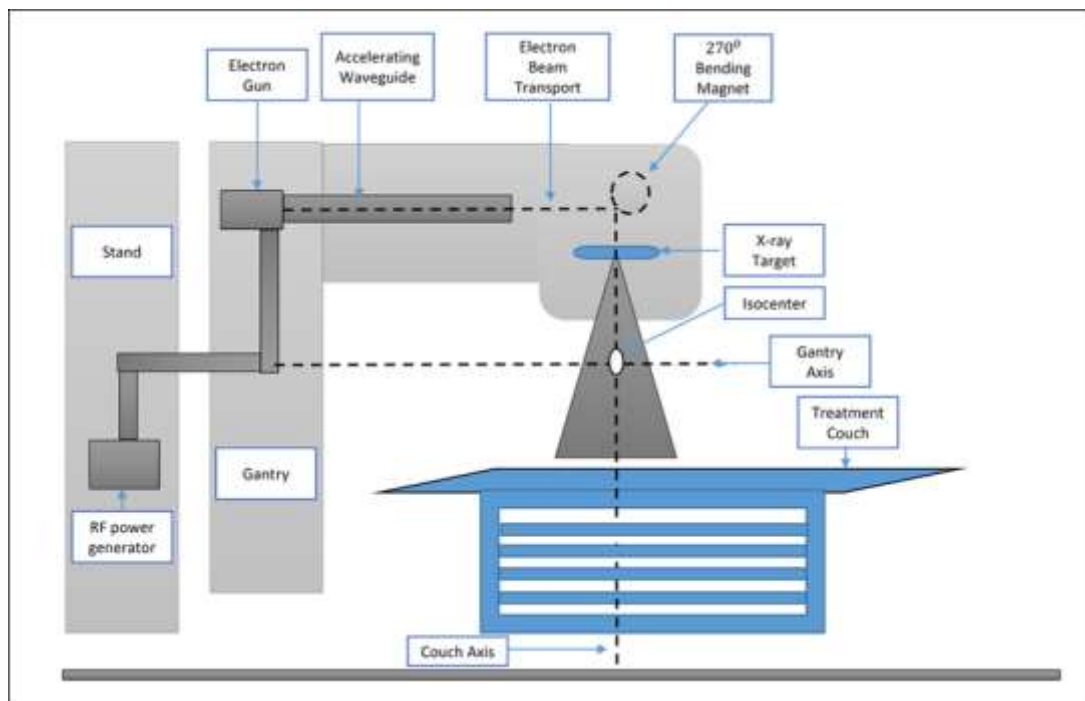


Figure 2.1 The schematic diagram of a linear accelerator (LINAC). The figure is adapted from (Saeed, 2015)

2.2 Radiotherapy Workflow

A systematic workflow in the radiotherapy department is a fundamental as any other department in the healthcare sector. To minimize the time consumed between the patients and the medical practitioners, an orderly workflow is essential since the schedule of treatment is very busy (Vieira, Demirtas, Van De Kamer, Hans, & Van Harten, 2019). The workflow of radiotherapy is categorized into 4 major steps which are firstly the diagnosis stage with the medical doctors, Secondly, is the treatment planning performed by a medical physicist, thirdly is pre-treatment verification, and lastly, the treatment delivery session which was carried out by radiotherapy technologist. The schematic diagram of radiotherapy workflow is illustrated in Figure 2.2

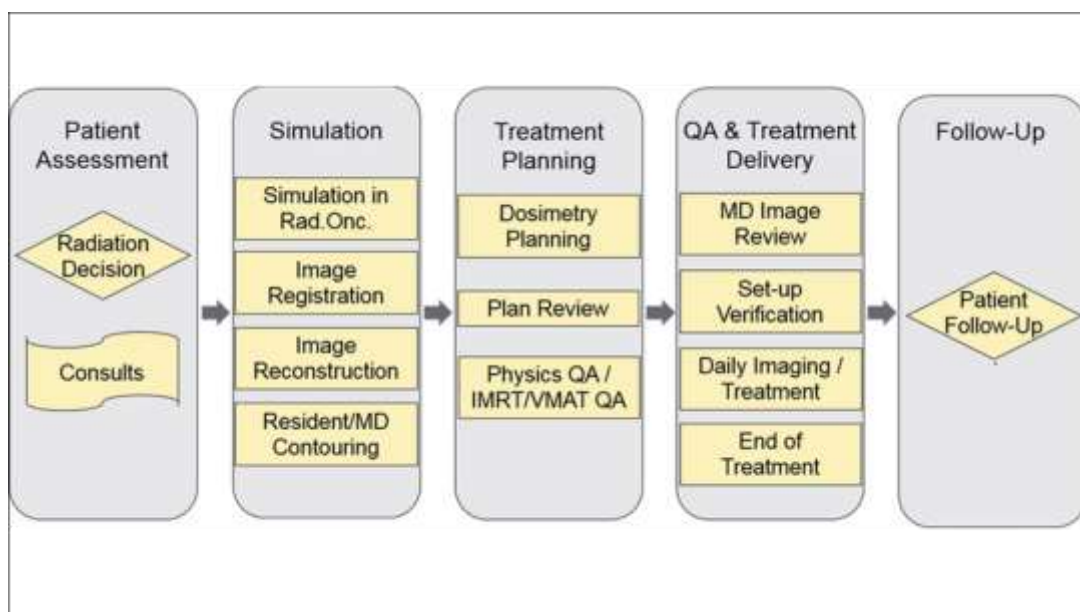


Figure 2.2 The schematic diagram of a radiotherapy workflow. The figure is adapted from (Osman, 2019)

2.2.1 Diagnostic Imaging: Simulation

The first step in the radiotherapy upon registration of the patient is the assessment of the patient's condition based on the results obtained from the imaging modalities by an oncologist or related medical doctors (Lencioni, Cioni, Della Pina,

Crocetti, & Bartolozzi, 2005). A patient that is transferred into the radiotherapy department will undergo a simulation process using the radiotherapy imaging modalities which is the Computed Tomography Simulation (CT-Simulation) as shown in Figure 2.3. This machine will help the medical practitioners to visualize the cancer location in the patient's body and any other complications related to cancer diseases. Then, from the CT datasets, the medical doctors will determine what amount of dose should be prescribed and then handled the case over to the medical physicist in charge for the next step in the treatment planning process. (Tino, Yeo, Leary, Brandt, & Kron, 2019)



Figure 2.3 The Phillips SPECT-CT in the Nuclear Medicine, Radiotherapy & Oncology Department, Hospital Universiti Sains Malaysia, HUSM

2.2.2 Treatment Planning

The radiotherapy treatment planning process is done using software designated specifically for planning treatment activities such as Eclipse, Oncentra, and a few other advanced programs such as Monaco as presented in Figure 2.4. In this process, the medical physicist will first contour the organ at risk (OAR) (Niroomand-Rad et al.) which are the crucial organs around the treatment area. After contouring the OAR, an oncologist will specify the plan target volume (PTV) which is where the tumor is

located, and other regions of interest (ROI) that are linked with the patient's case study. After that, the medical physicist will mark the point of interest through image registration (Dipasquale et al.) and other borders that affiliates with the treatment plan. Then, through the plan manager, beam insertion will be made and the factors that need to be considered during the beam insertion are the energy, field size, depth, the uses of the wedge, weighting factor, the isocentre location, the normalization point and also the gantry angles. When all the criterias fulfilled, the plan continues with dose prescriptions and fractions needed through consultation with the medical practitioners involved. Then, a complete plan with a prescribed dose is done and the treatment is ready to be tested in the next step of the pre-treatment verification process (Hoskin, 2019)

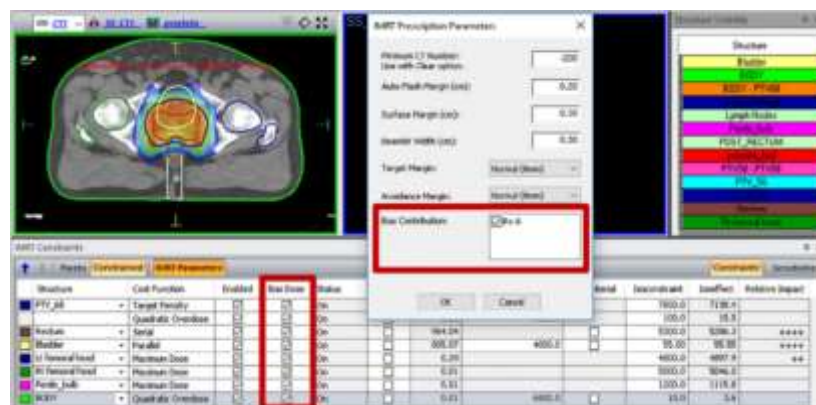


Figure 2.4 The tools in the Monaco treatment planning system. This figure is adapted from (Clements, Schupp, Tattersall, Brown, & Larson, 2018)

2.2.3 Quality Control: Pre-Treatment Verification

In clinical radiotherapy, treatment verification was performed to certify accurate dosimetry during clinical treatment delivery (Esplen, Therriault-Proulx, Beaulieu, & Bazalova-Carter, 2019). This quality control (QC) performed before the actual treatment is delivered to the patients, which to verify the input and output of the dose is the same and symmetric with the prescribed dose as planned. For example, the verification system with dosimeter used in this QC was Sun Nuclear equipment which

encompasses a gamma-index analysis software and the Arc Check phantom as depicted in Figure 2.5. Besides the software and phantom, this QC also required an ionization chamber and an electrometer. The set-up of the phantom is identical to the set-up of the real patients. When the verification of treatment and the plan were successfully executed, the treatment will be delivered to the patient.

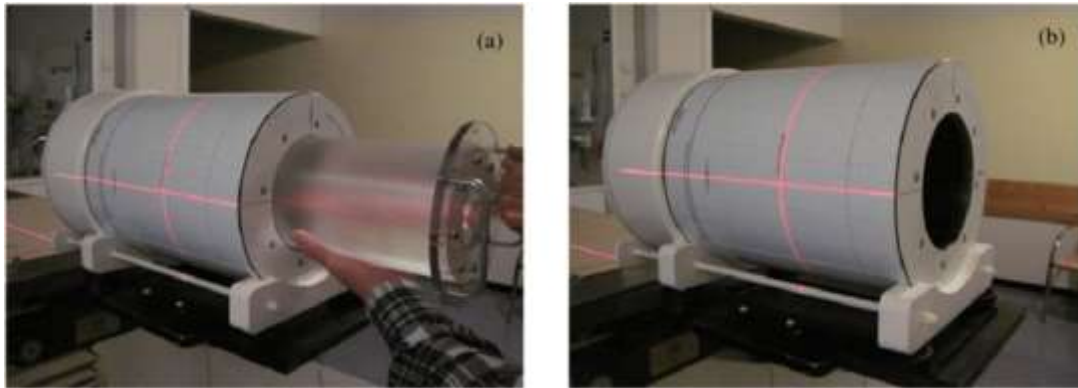


Figure 2.5 The ArcCheck phantom with (a) and without (b) optional cavity insert. This figure is adapted from (Petoukhova, Van Egmond, Eenink, Wiggenraad, & Van Santvoort, 2011)

2.2.4 Treatment Delivery

During this particular step in radiotherapy, the patient will have undergone the treatment where the tumor target will be bombarded with a high-energy photon or electron beam. The radiotherapy staffs will place the patients on the linear accelerator (LINAC) treatment couch and they are responsible for the patient's care as shown in Figure 2.6. The placement of patients is based on the treatment plan created and any immobilization devices such as a headrest, chest board, or bolus may be utilized during treatment, if necessary. The comfort of the patients is essential for better treatment since movement is prohibited during the irradiation process. To ensure the efficiency and accuracy of the radiation dose to the patient during treatment, a thorough study on the dosimetry is vital. This investigation is needed to give promising therapeutic outcomes to the patients for their better health.



Figure 2.6 The cancer patients on the Varian LINAC treatment couch in the Nuclear Medicine, Radiotherapy & Oncology Department, Hospital Universiti Sains Malaysia, HUSM

2.3 Radiotherapy dosimetry

Modern radiotherapy relies on accurate dose delivery to the target, and the accuracy must be within $\pm 5\%$. Hence, to achieve this consistent accuracy, the output of LINAC must be calibrated regularly using ionization chambers and other dosimeters according to the standard references. Associated with primary standard calibration itself, the radiation dosimeter used together with the phantom also needs to be properly calibrated. The common types of dosimeters available for radiotherapy dosimetry are ionization chamber (IC), radiochromic films, thermoluminescence detectors (TLDs), optically stimulated luminescence (OSL), and several other types of dosimeters (Seco, Clasio, & Partridge, 2014). In radiotherapy dosimetry, there are a few advantages and disadvantages of the dosimeters related to the dose measurements and other parameters depending on their characteristics (Niroomand-Rad et al., 1998).

2.3.1 Ionization chamber (IC)

IC is a standard dosimeter for radiotherapy dosimetry and must be calibrated from Primary Standards Dosimetry Laboratory (PSDL) or Secondary Standards Dosimetry Laboratory (SSDL). IC is mostly being used in dosimetry protocol such as the IAEA TRS-398 Code of Practice to verified the output and input of a medical LINAC through quality assurance standard operation procedure (SOP) for the determination of dose. The IC comes in many shapes and sizes relating to the specific requirements such as cylindrical (thimble type) IC or Farmer type chamber which the name is based on the shape of the chamber sensitive volume itself that mimics a thimble. Parallel-plate IC is used for surface dose measurement in the build-up region of MV photon and electron beam dosimetry of energy below 10 MeV. Other types of IC which are brachytherapy chambers also one of the customary types of IC found in the dosimetry field. This type of chamber is definitely for appertaining in brachytherapy dose measurement.

In general, the IC is designed with a gas-filled cavity surrounded by a conductive outer wall and it has a central collecting electrode. The wall and collecting electrode are separated with a high-quality insulator to reduce the current leakage when a polarizing voltage was applied to the chamber. The charge produces inside the air cavity of IC when strike by radiation is measured using a device called an electrometer. (Fares et al., 2020; Patel, Majumdar, Vijiyan, & Hota, 2005; Reis & Nicolucci, 2016). The picture of the IC is manifest in Figure 2.7



Figure 2.7 The figure of the cylindrical ionization chamber. This figure is adapted from www.flukebiomedical.com

2.3.2 Radiochromic Film

The disclosure of x-ray was first introduced by Roentgen in 1895 using a photographic film as a medium to measure the radiation. This type of radiation detector is a relative dosimeter that acts like a display device and an archival medium. Present radiographic film or x-ray film is typically encompassing a suspension of silver bromide (AgBr) grains, with up to 10% silver iodide suspended in a matrix (Seco et al., 2014). When radiographic film hit by radiation, silver bromide ionization will developed, and then radiation interaction will produce a latent image in the film. Then, after processing the image becomes visible, which is the inauguration of the film overexposed due to air gap and this state of film is permanent. The different level of darkening of the film indicates different intensity and range of energy of the light transmission. The light transmission is a function of film opacity, and film opacity can be measured in terms of optical density (OD) using a densitometer. At the same time, OD is a function of dose.

The film dosimetry was then upgraded with the instigation of a range of polydiacetylene-based radiochromic or GafChromic film (GAFCHROMICTM, International Specialty Products, Wayne, NY, USA) (Seco et al., 2014). This radiochromic type of film is a transparent film that develops blue color upon radiation

exposure. These changes are because the films contain a special dye that polymerized upon radiation exposure. These radiochromic films have a few competent characteristics which make them very acceptable and useful for radiotherapy dosimetry and quality assurance. Among the criteria are weak energy dependence, high spatial resolution, self-developing, grainless, and near tissue equivalence (Seco et al., 2014). The tissue equivalence property of the film is composed of 9.0% hydrogen, 60.6% carbon, 11.2 % nitrogen, and 19.2% oxygen in specific (Ismail et al., 2009). The expediency of the GafChromic films compared to radiographic are easy to use, no need for a darkroom, films cassette of film processing, dose-rate independence, better energy attribute except for low energy x-rays which is less than 25 kV (kilovoltage), insensitive to ambient conditions such as humidity, and useful at higher doses (Butson, Cheung, & Yu, 2004; Evans, Devic, & Podgorsak, 2007).

Historically the standard tool for quality assurance of IMRT or other radiotherapy quality assurance (Alqathami et al.) programs has been a radiographic film but recently the latest version of radiochromic films has been applied. The GafChromic EBT3 film is a type of radiochromic film to measures absorbed doses of radiation in a two-dimensional plane. The GafChromic EBT3 variant of usage was mainly designed for high-energy beams in the megavoltage range of up to 10 Gy. Among the advanced specifications proposed by this latest GafChromic EBT3 film compared to the previous one is that it has a good response at high-dose level, energy, and dose rate independence while demonstrating better energy characteristic (Borca et al., 2013). A study by Park et al., in 2017 has proven that the application of the 3D-printed bolus verified by the assessment of the percentage depth dose (PDD) profiles by maneuvering the GafChromic EBT3 film which was crop and placed along the vertical direction in phantom. The assessment was compared with and without the bolus alongside the

standard Superflat bolus (Park, Oh, Yea, & Kang, 2017). Figure 2.8 shows an example of a GafChromic film irradiated at different doses.

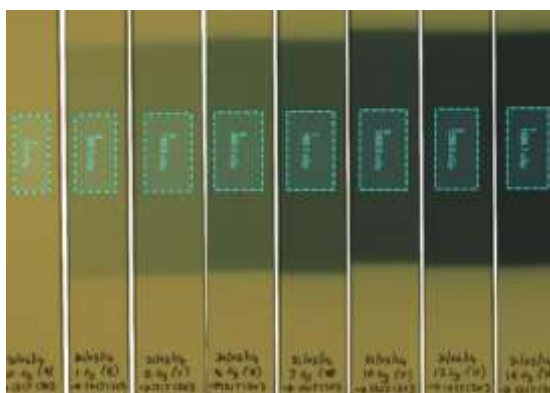


Figure 2.8 The figure of irradiated radiochromic film calibration strips (film batch lot b=#12171303). This figure is from (Palmer, 2015)

2.3.3 Thermoluminescence Detector (TLD)

A thermoluminescent detector (TLD) is a radiation dosimeter that is commonly used in radiotherapy dosimetry. This dosimeter can absorb radiation and release it back in terms of the final reading which is the thermoluminescence signal in micro Coulomb (μC). Measuring absorbed dose in the surrounding area is certain by using TLD due to its straight radiation captured however for biological dose measurements, there had been an issue regarding the LET-dependent enhancement of the relative biological effectiveness (RBE) (Olko, 2010). Besides, the TLD also being widely used in Monte Carlo radiation dosimetry on brachytherapy procedures and the TLD is used in collecting point dose throughout the experiments (Lymperopoulou et al., 2005).

Since the application of the luminescence detector is well-established in radiation dosimetry study, hence this kind of detector was decided to be implemented in dosimetry characterization on the phantoms in this research which also acts as an alternative method besides the GafChromic EBT films. In dosimetry studies, the TLD-100 and TLD-100H are frequently being used and both were in chip design which has

the size of $5.0 \times 5.0 \times 0.6 \text{ mm}^3$ (Yang, Wang, Townsend, & Gao, 2008). Besides the design of the chip, TLD also available in powder, rods, and ribbon. Since the TLD's shape and size are small, it is chosen to be used by radiation workers and practitioners as their annual dose limit radiation detector in a pocket dosimeter shape. The figure of TLD is as shown in Figure 2.9

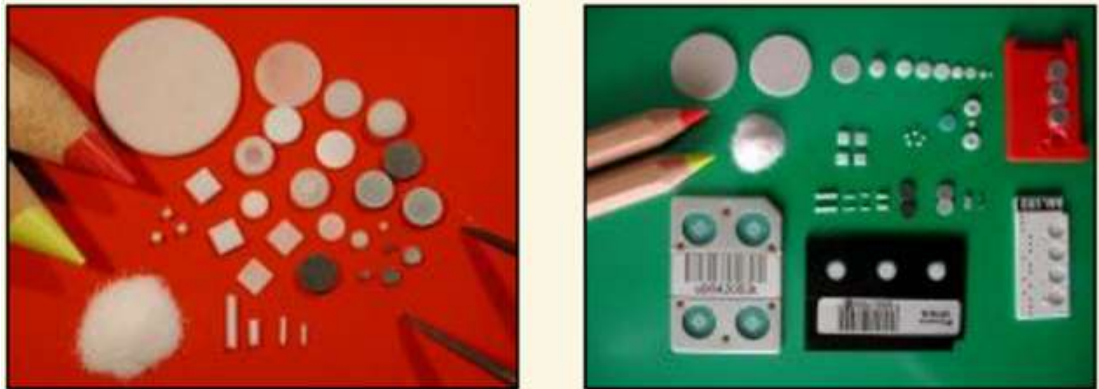


Figure 2.9 The figure of thermoluminescence detector chips in different sizes and shapes. This figure is from <http://www.tld.com.pl/tld/index.html>

2.3.4 Optically Stimulated Luminescence (OSL)

The optically stimulated luminescence (OSL) detector is another type of luminescence dosimeter used for radiation dosimetry. OSL works on the similar fundamental principle as TLD but the only difference is the readout technique that is performed by a controlled illumination by the detector instead of heating as applied by TLDs (Yukihara & McKeever, 2008). The OSL is being experimented to be in mobile and lightweight design which this type of radiation detector is extensively used by radiation workers as personal dosimeter because of its small sizes, reusable properties and allow real-time dose measurements for in-vivo manipulation. The OSL is generally composed of a thin layer of $\text{Al}_2\text{O}_3:\text{C}$ which has a thermoluminescence sensitivity 50 times larger than TLD-100 which comes in the lithium fluoride doped

with magnesium and titanium, LiF: Mg, Ti (Bøtter-Jensen, Thomsen, & Jain, 2010; Ristic, 2013).

Besides being used as a personal dosimeter by radiation health personnel, the OSL is also being studied and used in space radiation dosimetry (Yukihara et al., 2006). There are tremendous studies related to OSL potential in radiation dosimetry due to its accuracy in measuring radiation dose when compared to other dosimetry which needs some corrections after readout (Bulur, 1996). The OSL is exemplified as shown in Figure 2.10

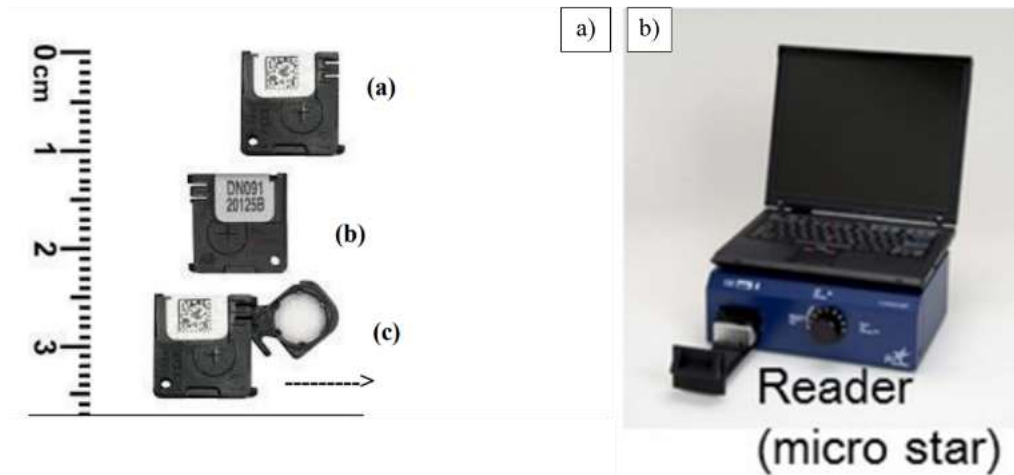


Figure 2.10 The optically stimulated luminescence detector (a) and OSL reader (b). This figure is from (Okino et al., 2016; Remley, 2017)

2.3.5 Other Types of Dosimeter

Besides all the commonly used radiation dosimeters mention in the previous section, other types of dosimeters are available for radiotherapy dosimetry which are semiconductor dosimeter, metal-oxide-semiconductor field-effect transistor (MOSFET), diamond dosimeter, gel dosimetry system, alanine or electron paramagnetic resonance dosimetry system, and plastic scintillator dosimetry system. The semiconductor dosimeter is a positive-negative silicone diode dosimeter which when exposed to radiation, the charged particles inside the thin depleting layer will set

free and allowed the signal current to flow. MOSFET dosimeter works on the principle where the ionizing radiation inside the silicone oxide will generate charges, then the charges will move forward which leads to a changing in threshold voltage between materials of the dosimeter. The readout of this type of dosimeter is based on its previous history of the measured signal and unfortunately, it showcases a temperature dependence (IAEA,). (Rajan, 2016)

Meanwhile, the diamond dosimeter is a type of dosimeter that can change resistance upon radiation exposure and be designed to measure relative dose distributions in high-energy photon and electron beams. It is based on a natural diamond crystal property which is sealed in a polystyrene housing. Next, gel dosimetry is broadly used in 3D dosimetry which satisfies the relative dose measurements and operates with a phantom that capable of measuring the absorbed dose distribution in a full 3D geometry. This sort of dosimetry is tissue-equivalent and flexible in shape and sizes and the dosimeter that belongs in this group is the Fricke gel, polymer gel, and presage gel. Then, for alanine dosimetry, the name itself refers to one of the amino acids that compressed in the form of rods or pellets with an inert binding material and are also a tissue-equivalent material. (IAEA) (Rajan, 2016)

Another type of radiotherapy dosimeter is the plastic scintillation dosimetry which is made in very small size about 1 mm^3 or less. Despite its size, this dosimeter gives adequate sensitivity for clinical dosimetry, and hence they are being used in a high spatial resolution case such as within high dose gradient regions. Lastly is the SMART dosimeter which is used for advanced radiation therapy dosimetry. (IAEA) (Rajan, 2016). One type of SMART dosimeter is emphasized in Figure 2.11 which is a double-stack SMART dosimeter. This SMART type of dosimeter is design with gold

nanoparticles (AuNps) doped compartment (clear) and an undoped compartment (dyed yellow). The same double-stack SMART dosimeter is shown in Figure 1.11 (a') as after exposure of half of it to ultraviolet radiation, it is showing that the radiation-induced change in optical density. A transparent yellow dye was added to the undoped compartment to allow the 2 compartments to be visually distinguished. The other type of SMART dosimeter also has the actual cylinder-in-cylinder which was analyzed in the study by Alqathami et al., 2012.

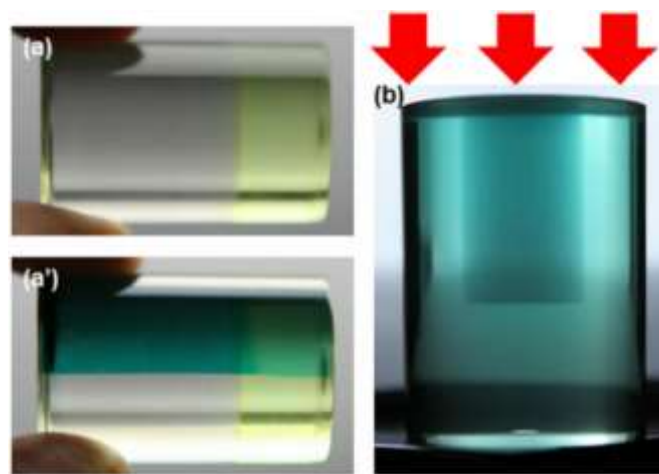


Figure 2.11 Different Sensitivity Modulated Advanced Radiation Therapy (SMART) dosimeter designs. (a) A double-stack SMART dosimeter design with a gold nanoparticles (AuNps) doped compartment (clear) and undoped compartment (dyed yellow). (a') The same double-stack SMART dosimeter after exposure of half of it to ultraviolet radiation, showing the radiation-induced change in optical density. A transparent yellow dye was added to the undoped compartment to allow the 2 compartments to be visually distinguished. (b) The actual cylinder-in-cylinder SMART dosimeter was analyzed in this study after irradiation. Red arrows indicate the direction of irradiation.). This figure is from (Alqathami et al., 2012)

2.4 Radiotherapy Phantom

In radiotherapy, various types of the phantom are available for different purposes and often addressed as radiotherapy phantoms (RPs). Radiotherapy phantoms (RPs) are categorized into three groups, first is the homogenous phantoms such as solid water phantom, next is the heterogeneous phantoms such as CT-ED, slabs with different density rods and the third category is the anthropomorphic such as commercialize

Alderson RANDO® phantom and recently based on additive manufacturing-Rps (AM-RPs) (Tino et al., 2019). The current existing phantoms either homogenous or heterogeneous, are designed to be tissue equivalent but most of them did not mimic 100% as human body inhomogeneity and density. Theoretically, the materials of choice to be a tissue or water equivalent for phantom must pose similar effective atomic number, number of electrons per unit gram, and mass density that suit the Compton scattering effect as it was the most prominent type of interaction in the clinical range of megavoltage beam in radiotherapy. (Khan & Gibbons, 2014).

There is a fully human-body-like phantom that being produce successfully and commercially nowadays, such as the Alderson RANDO® phantom (The Phantom Laboratory, Salem, NY, USA) (Park et al., 2017). The Alderson RANDO® phantom in its eldest edition was recognized as the Alderson Radiation Therapy (ART) phantom, and the ART phantom has been strained and ameliorates in both patterns and materials. Equally important that the RANDO® phantoms are generally molded of tissue-equivalent materials, and they are designated within highly sophisticated technology constraints and follow ICRU-44 (International Commission on Radiation Units and Measurements) standards (RSD Radiological Support Devices INC, 2018). There are male and female RANDO® phantoms that currently available, and they are different in height and weight which 175 cm (5 ft. 9 in.) and 73.5 kg (162 lb.) for male while 155 cm (5 ft. 1 in.) and 50 kg (110 lb.) for a female phantom. Additionally, these phantoms are transected horizontally into 2.5 cm thick slices, and each slice has holes for dosimeter placement slots (RSD Radiological Support Devices INC, 2018). The holes fabricated in the phantom are particularly for thermoluminescence detector (TLD) placement and other dosimeters that have the same size as TLD. Furthermore, this type of phantom was made of real bones and organs, which mimics the different densities in

the human body (tissue-equivalent). Besides, the RANDO® phantom comes with breast attachments of different sizes as integrated to different breast volumes. This phantom is very costly in production with only obtainable in standard shapes and design.

Besides, for the anthropomorphic phantoms, the sizes and shapes are only available in a healthy “standard” person which limited when compared with the real patient body. Furthermore, the limited uniformity between the phantoms if compared with the patient's body and organ will generate the dosimetry error. The solid water phantom, which is widely explicitly used in maintaining and regulates the radiation uniformity of the treatment area. A bolus is significant for the treatment of shallow tumors, increasing skin dose, and improving dose uniformity (Burlison, Baker, Hsia, & Xu, 2015). Besides these anthropomorphic commercial phantoms, there is a more advanced phantom called a patient-specific phantom through the process of additive manufacturing process (AM) which falls in the category of the anthropomorphic additive manufacturing radiotherapy phantoms (AM-RPs). The production of the standard type of patient-specific phantom is in very complex ways and consumes a handy cost that is mainly produced from the 3D process. The summary of radiotherapy phantoms is illustrated in the schematic diagram as in Figure 2.12

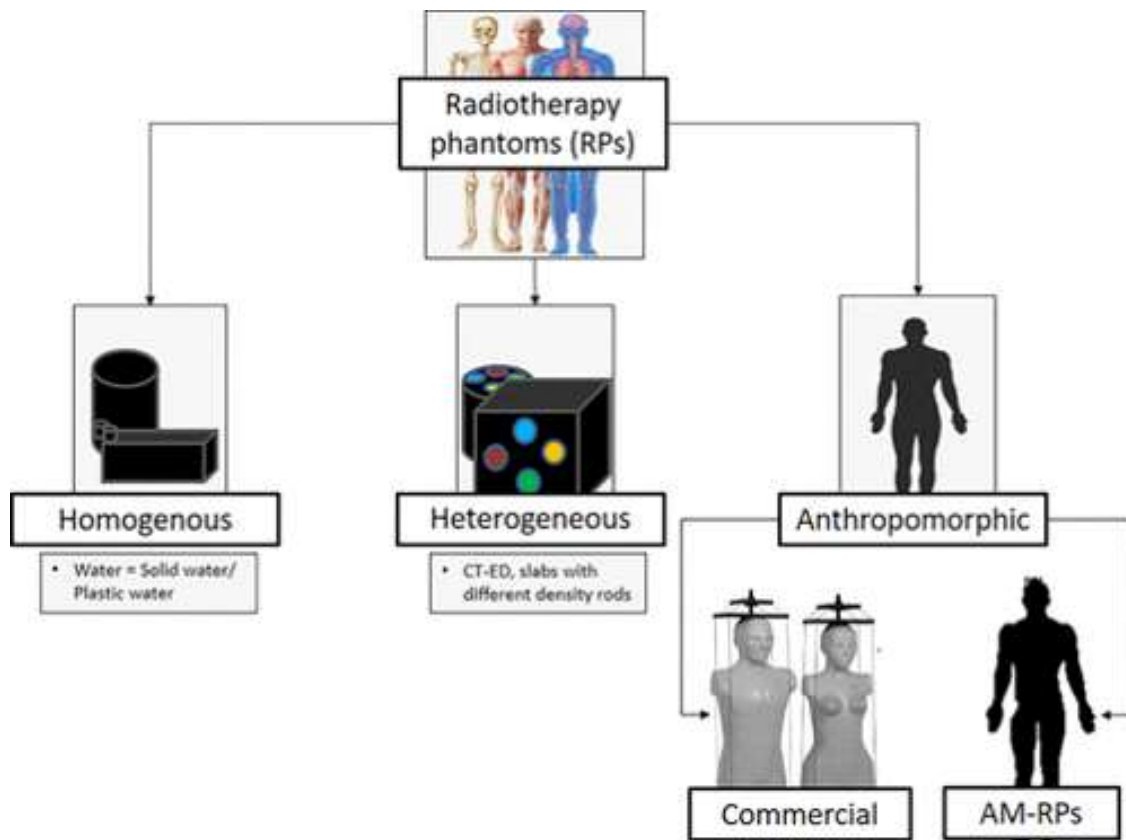


Figure 2.12 The figure of radiotherapy phantoms in different sizes and shapes depending on their category. This figure is from (Tino et al., 2019)

2.5 Introduction to 3D Printing

3D printing or additive manufacturing (AM) technologies have been broadly used in the industrial and clinical fields. Most products manufacturing nowadays are being created by using a 3D printing technique since it was printed from a custom-made approach and not just stick to one basic or standard shape which indicates that the choices are unlimited. The available shape or custom shape can be created online using available free 3D software or the subscribed one and the created shapes can simply have transferred online to any 3D printing software to proceed with the manufacturing of the products. Hence, with the easy and unlimited excess of the 3D software and 3D printing materials online, this 3D method surely is the choice made by most products manufacturing. The evolution of information technology (IT) has been connected with 3D printing simultaneously which made 3D printing more practicable and accessible

through the IT streams. The availability of 3D scans, 3D editing, and 3D print materials and information is simply through any online browsing platform. The generated three-dimensional object from a computer-aided design (CAD) model or any digital 3D model is infinite in the terms of its design, shape, sizes, and types. The CAD software is also numerous in quantity which was designed by expertise in software engineering and the accessibility of the software are some free access and some are through subscriptions. (Barnatt, 2014)

The materials applied in 3D printing technology also vary in their properties, strength, durability, flexibility, heat resistance, biocompatibility, biodegradability depending on the purposes of the printing end-product produced. Hence in the medical field, the ones that are closed to water-equivalent such as Acrylonitrile Butadiene Styrene (ABS), polylactic acid (PLA), or resin-based materials were chosen as the materials used in 3D printing of phantom as the phantom is an object to replace the human body. The fundamentals and applications of 3D printing used novel materials were assigned in a few basic classifications of smart materials, ceramic materials, electronic materials, biomaterials, and composites (Dawood, Marti, Sauret-Jackson, & Darwood, 2015) The Figure 2.13 represented a type of 3D printer machine.

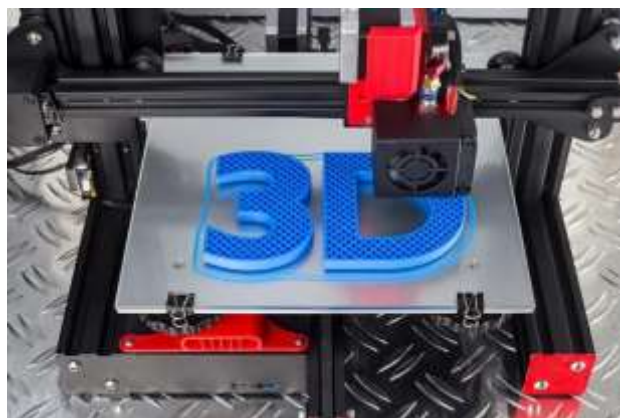


Figure 2.13 The figure of a type of 3D printer available online. This figure is from <https://www.forbes.com>

2.6 Additive Manufacturing (AM) Radiotherapy Phantoms (AM-RPs)

In modern radiotherapy technologies, researchers have developed and improved the phantom's manufacturing technique by using additive manufacturing (AM) or known as 3D printing. The anthropomorphic phantoms were developed for myriad functions in radiotherapy with different body parts, anatomical details, and materials. The generation of the 3D printed phantom is normally acquired from medical image data such as CT scan, MRI, PET, and SPECT. The imaging data from the clinical radiological machine is saved in DICOM format and computationally transform in 3D mesh and STL file format before being sent to the 3D printer for production (Rengier et al., 2010). Figure 2.14 shows the process chain in the production of a 3D printed prototype model.

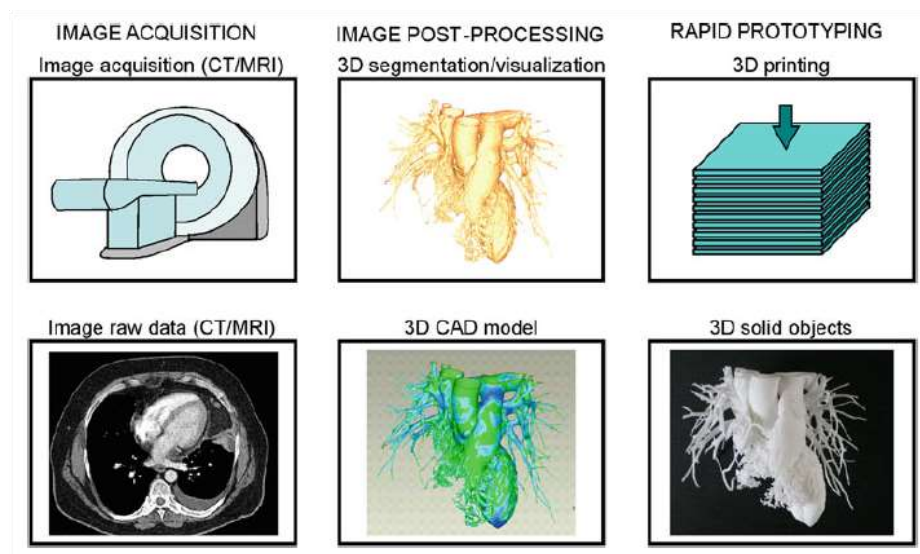


Figure 2.14 The methods in the production of 3D printed prototype model (Rengier et al., 2010)

The anatomical details, especially for radiotherapy phantom, are commonly obtained from CT image data to build a patient-specific phantom (Kamarul et al, Craft et al, Ehler et al Izzo et al, and Kamomae et al). The 3D images from patients' CT were extracted and 3D printing techniques were used to fabricate the phantom. (Kamarul A Abdullah, Mark F McEntee, Warren Reed, & Peter L Kench, 2018; Craft & Howell, 2017; Ehler, Barney, Higgins, & Dusenbery, 2014; Izzo et al., 2016; Kamomae et al., 2017). Kamomae et al have developed 3D printed patient-specific phantom for artificial in vivo dosimetry in radiotherapy quality assurance. A standard anthropomorphic head phantom containing bone and the nasal cavity was scanned using a CT scanner and the data were used to construct the 3D printed head phantom. Comparison between the standard and 3D printed phantom showed agreeable results in terms of dosimetric properties (Kamomae et al.). Craft and Howell 2017 have converted a postmastectomy patient's clinical CT DICOM data into a 3D model and then printed the phantom into eleven 2.5 cm thick sagittal slices. The full-scale patient-specific phantom has been fabricated with high accuracy with minimal material warping error (Craft & Howell). The printed phantom and the actual patient show excellent agreement as shown in Figure 2.15. Yea et al. have also investigated the feasibility of a 3D-printed anthropomorphic patient-specific head phantom for patient-specific quality assurance of intensity-modulated radiotherapy. CT images of the patient's head were used for phantom fabrication with anatomical structures such as the oral cavity, nasal cavity, and larynx were left as cavities (Yea et al, 2017). Dosimetric verification also showed comparable results with the established QA procedure. The phantom is shown in Figure 2.16